Since January 2020 Elsevier has created a COVID-19 resource centre with free information in English and Mandarin on the novel coronavirus COVID-19. The COVID-19 resource centre is hosted on Elsevier Connect, the company's public news and information website.

Chemical Engineering Journal 404 (2021) 127105

Contents lists available at ScienceDirect

Chemical Engineering Journal

journal homepage: www.elsevier.com/locate/cej

Electrostatic self-assembly enabled flexible paper-based humidity sensor with high sensitivity and superior durability

Penghui Zhu [a,e,f], Yudi Kuang [b,c,d], Yuan Wei [a,e], Fang Li [a,e], Huajie Ou [a,e], Feng Jiang [f,*], Gang Chen [a,e,*]

[a] State Key Laboratory of Pulp and Paper Engineering, South China University of Technology, Guangzhou 510640, China
[b] School of Biomedical Science and Engineering, South China University of Technology, Guangzhou 510006, China
[c] National Engineering Research Center for Tissue Restoration and Reconstruction (NERC-TRR), Guangzhou 510006, China
[d] Innovation Center for Tissue Restoration and Reconstruction, South China University of Technology, Guangzhou 510006, China
[e] Guangdong Engineering Technology Research and Development Center of Specialty Paper and Paper-Based Functional Materials, South China University of Technology, Guangzhou 510640, China
[f] Sustainable Functional Biomaterials Lab, Department of Wood Science, University of British Columbia, Vancouver V6T 1Z4, Canada

ARTICLE INFO

Keywords:
Humidity sensor
Electrostatic self-assembly
High sensitivity
Superior durability
Respiration monitoring

ABSTRACT

Humidity sensors have been widely used for humidity monitoring in industrial fields. However, the application of conventional sensors is limited due to the structural rigidity, high cost, and time-consuming integration process. Owing to the good hydrophilicity, biodegradability, and low cost of cellulose, the sensors built on cellulose bulk materials are considered a feasible method to overcome these drawbacks while providing reasonable performance. Herein, we design a flexible paper-based humidity sensor based on conductive 2,2,6,6-tetramethylpiperidine-1-oxyl (TEMPO)-oxidized cellulose fibers/carbon nanotubes (TOCFs/CNTs) conformal fibers network. The CNTs are dispersed by cationic cetyl trimethyl ammonium bromide (CTAB), which introduces positive charges on the CNTs surface. The conductive fibers are achieved by an electrostatic self-assembly process that positively charged CNTs are adsorbed to the surface of negatively charged TOCFs. The vast number of hydrophilic hydroxyl groups on the surface of TOCFs provide more water molecules adsorption sites and facilitate the electron transfer from water molecules to CNTs, endowing the sensor with an excellent humidity responsive property. Besides, the swelling of the TOCFs greatly damages the conductive CNTs network and further promotes the humidity sensitive performance of the sensor. Benefiting from the unique structure, the obtained sensor exhibits a maximum response value of 87.0% ($\Delta I/I_0$, and the response limit is 100%), outstanding linearity ($R^2 = 0.995$) between 11 and 95% relative humidity (RH), superior bending (with a curvature of 2.1 cm^{-1}) and folding (up to 50 times) durability, and good long-time stability (more than 3 months). Finally, as a proof of concept, the sensor demonstrates an excellent responsive property to human breath, fingertip humidity, and the change of air humidity, indicating a great potential towards practical applications.

1. Introduction

In recent years, with the rapid growth of intelligent technology such as the internet of things and human–machine interface, a variety of devices have been developed for air quality monitoring [1–4], disease screening and diagnosis [5–8], human motion detecting [9–11], and so on. Humidity is one of the essential indexes of air, which is important for industrial and agricultural production and our daily life. As a humidity detection tool, flexible electronic humidity sensors have attracted much attention because of their wide applications in fields of wearable electronics, smart textiles, electronic skin, and soft robotics [12–20]. Specifically, conductive polymer composite-based humidity sensors with incorporated electrically conductive fillers in insulating polymer matrixes are attracting much attention owing to their excellent flexibility, low cost, and ease of processing [21–27]. A range of polymers, such as poly (ethylene terephthalate) [28,29], poly (ethylene-co-vinyl acetate) [30], polyimide [31–33], poly (ethyleneimine) [34], poly (vinylidene fluoride) [35], and silicone rubber [36], have been demonstrated as platforms for the preparation of flexible humidity sensors. However, these petroleum-based polymers are

* Corresponding authors.
E-mail addresses: feng.jiang@ubc.ca (F. Jiang), papercg@scut.edu.cn (G. Chen).

https://doi.org/10.1016/j.cej.2020.127105
Received 28 May 2020; Received in revised form 4 August 2020; Accepted 20 September 2020
Available online 24 September 2020

nonbiodegradable that inevitably pose negative impacts on the environment. To address this issue, many efforts have been dedicated to applying biodegradable polymers, including poly(vinyl alcohol) [37–40], polylactic acid [41], and chitosan [42,43], as the matrix for flexible humidity sensors, while these polymers suffer from poor durability under high humidity conditions due to their partially water solubility, leading to materials destruction and deterioration of the function of the sensors.

Cellulose, the most abundant natural polymer on earth, is considered as an ideal candidate for preparing humidity sensors because of its excellent hydrophilicity, biodegradability, biocompatibility, and low cost [44–49]. The mass hydroxyl groups on cellulose chains interact with each other, forming dense hydrogen bonding networks, which result in the insolubility of cellulose in most solvents including water [23,50]. In terms of conductive fillers, carbon-based materials are promising candidates owing to their high conductivity, electrical sensitivity, and stability [51–56]. As typical carbon-based materials, carbon nanotubes (CNTs) offer good humidity sensitivity given their p-type semiconductor properties, high aspect ratio, nanoscale hollow structure, and excellent mechanical properties [57–60]. Thus, tremendous efforts have been devoted to integrating CNTs with cellulose for the design of humidity sensors, which can be classified into three categories. (1) Embedding CNTs into regenerated cellulose matrix to obtain sensors in forms of fiber, film, or aerogel [50,61]. These sensors can convert the change of humidity into visual electrical signals rapidly, but the strong base (7 wt% NaOH) and low temperature (-12 ℃) were generally required in dissolving cellulose, leading to a relatively lower producing efficiency. Also, the sensitivity was lower than 61.0%. (2) Blending CNTs with cellulose nanofiber (CNF) to form the CNF/CNT dual networks, where CNTs functioned as the conductive material, and CNF served as the dispersant for CNTs and humidity sensitive material [62]. The excellent affinity to water vapors of CNF enabled the senor with

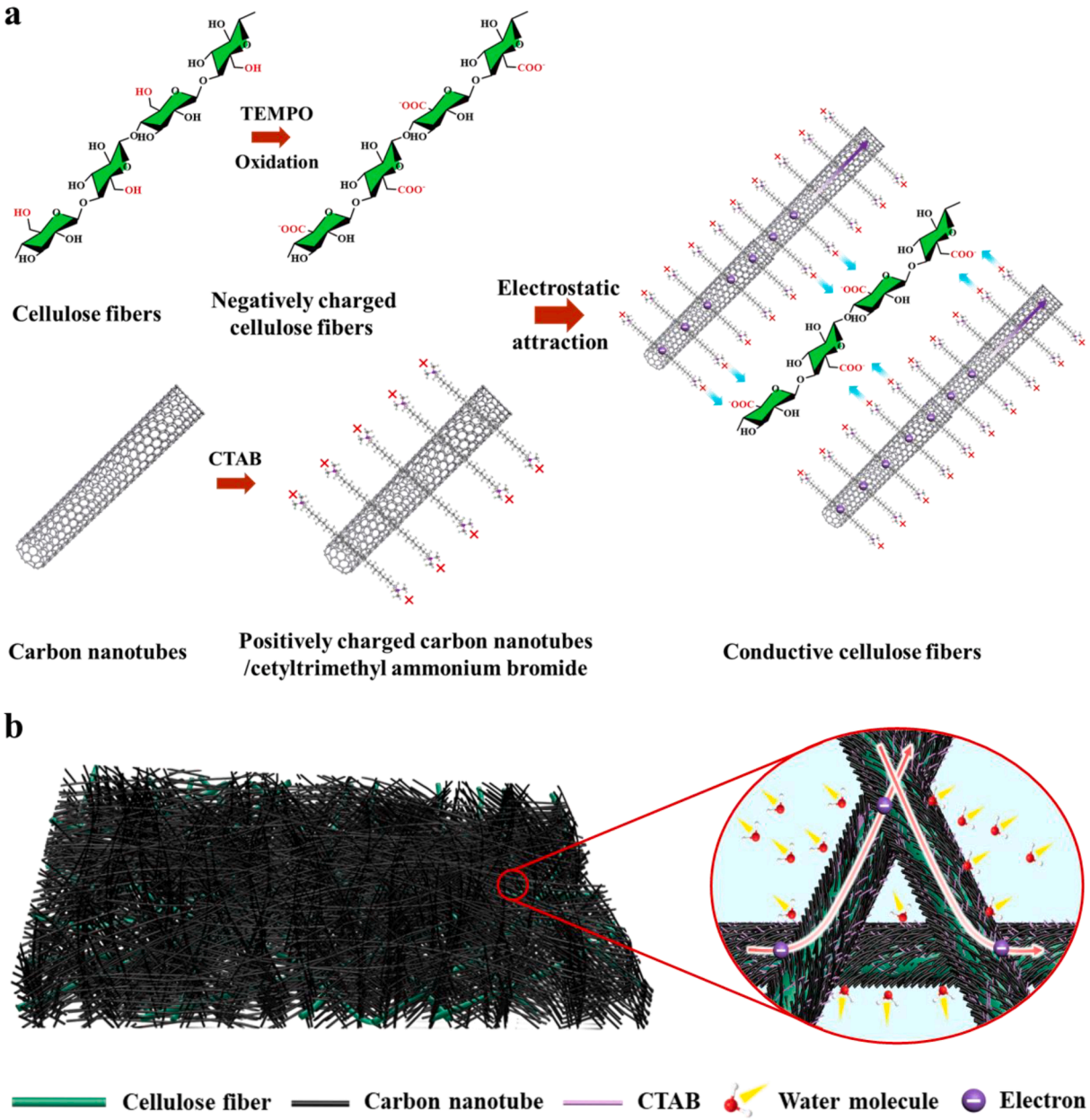

Fig. 1. Schematics illustrating the formation mechanism of the conductive cellulose fibers and the fibers network structure of the obtained paper sensor. (a) Schematic illustration of the preparation of conductive cellulose fibers by electrostatic attraction of negatively charged TOCFs and positively charged CNTs. (b) Schematics illustration of the network of the paper sensor based on the conformal conductive TOCFs/CNTs fibers.

enhanced humidity sensitive performance. However, due to the limited dimension change of the CNF network under humidity conditions, the improvement in sensitivity was still limited (lower than 70%). Meanwhile, the stability of the sensor was also unsatisfied for the practical applications. (3) Depositing CNTs onto the surface of cellulose paper to prepare sensors with bilayer structure. The cellulose paper layer acted as water molecules reservoir and supporting substrate in this design [63–65]. However, the electrical signal variation of conductive CNTs networks arising from the swelling of cellulose fibers was insignificant since most CNTs adhered to the paper surface, which resulted in a relatively low humidity response of the paper sensors (lower than 65%). Despite these achievements in cellulose-based humidity sensors design, these sensors still face some major challenges including strict synthesis technology and equipment as well as inadequate humidity sensitive performance. As a result, a universal and easy to scale-up strategy for high-performance cellulose-based humidity sensors remains arduous.

In this work, we developed a flexible paper-based humidity sensor based on conductive 2,2,6,6-tetramethylpiperidine-1-oxyl (TEMPO)-oxidized cellulose fibers (TOCFs)/CNTs network. The conductive fibers were achieved by an electrostatic self-assembly process that positively charged CNTs were adsorbed to the surface of negatively charged TOCFs, as shown in Fig. 1a. Microsized cellulose pulp was pretreated by the TEMPO oxidization process, in which the C6-hydroxyl groups on cellulose chains were selectively oxidized to carboxyl groups, leading to strong negatively charged cellulose fibers. In addition, CNTs were dispersed in water with cetyl trimethyl ammonium bromide (CTAB) as a surfactant by sonication. Cationic CTAB micelles were formed on the surface of the CNTs and positively charged CNTs were then obtained. Negatively charged TOCFs can firmly adsorb positively charged CNTs by electrostatic attraction, forming a conformal conductive fibers network. The CNTs function as a conductive filler and humidity sensitive material for water molecules exchange between the conductive network and the external environment, while the functions of the TOCFs include: (1) supporting conductive CNTs to form a flexible paper; (2) amplifying the humidity change signal (current change) by increasing the volume change of the conductive CNTs network due to its easy swelling behavior after adsorbing water molecules under humidity conditions; and (3) providing more adsorption sites as water molecules acceptors and facilitating the electron transfer from water molecules to CNTs (Fig. 1b). With this unique structural design, the adsorbed water molecules and hygroscopic expansion of TOCFs are fully exploited for humidity sensing. Consequently, our sensor achieved high humidity response (up to 87.0%, and the response limit is 100%), excellent linearity (R^2 = 0.995), superior bending (with a curvature of 2.1 cm^{-1}) and folding (up to 50 times) durability, and good long-time stability (more than 3 months).

2. Experimental section

2.1. Materials

Bleached hardwood pulp was supplied by Lee & Man Paper Manufacturing Co., Ltd (Chongqing, China). TEMPO was purchased from Sigma Aldrich (Saint Louis, USA). Sodium bromide (NaBr) was obtained from Kemiou Chemical Reagent Co., Ltd (Tianjin, China). Sodium hypochlorite (NaClO) was purchased from Fuyu Fine Chemical Co., Ltd (Tianjin, China). Commercially available carboxylated multi-walled CNTs (greater than 95 wt% purity; carboxyl content: 2.00 wt%) were obtained from Nanjing XFNANO Materials Tech Co., Ltd. (Nanjing, China). The CNTs are 0.5–2 μm in length and 10–20 nm in diameter. CTAB was purchased from Macklin Biochemical Co., Ltd (Shanghai, China). Lithium chloride (LiCl) was purchased from Macklin Biochemical Co., Ltd (Shanghai, China). Calcium chloride ($CaCl_2$), potassium carbonate (K_2CO_3), sodium bromide (NaBr), sodium chloride (NaCl), and potassium nitrate (KNO_3) were purchased from Sinopharm Chemical Reagent Co., Ltd (Shanghai, China).

2.2. Preparation of TOCFs

TOCFs were prepared by the TEMPO oxidation system. Firstly, the bleached hardwood pulp (10 g) was dispersed into ultrapure water with a concentration of 2%. Next, TEMPO (0.16 g) and NaBr (1.03 g) were separately added into the pulp suspension, and the mixture was stirred continuously for 30 min at 800 rpm. Subsequently, NaClO (65 mL) was titrated into the above suspension to initiate the reaction. The pH of the system was kept constant at 10.5. After the reaction, the TOCFs were thoroughly washed with ultrapure water to remove the residual chemicals and then diluted to a concentration of 2%. The carboxyl content of the prepared TOCFs is 1.42 mmol/g.

2.3. Preparation of CNTs dispersion

CNTs were dispersed in water with CTAB as a surfactant. Firstly, CTAB powder (0.5 g) was added into ultrapure water (400 mL) under continuous agitation for 20 min. Then, CNTs powder (0.05 g) was added slowly into the obtained CTAB dispersion under bath sonication for 30 min. After sonication, the CNTs dispersion was further treated by an ultrasonic homogenizer (JY92-IIN, Scientz, China) for 20 min in an ice bath at a power of 650 W and 50% amplitude.

2.4. Preparation of conductive TOCFs/CNTs paper sensors

The conductive TOCFs/CNTs papers were obtained by assembling positively charged CNTs to the surface of negatively charged TOCFs through electrostatic attraction. Firstly, a certain amount of TOCFs suspension was mixed with CTAB-dispersed CNTs solution (50 mL) under magnetic stirring for 10 min to obtain a homogeneous TOCFs/CNTs suspension. By adjusting the amount of TOCFs added to the CNTs solution (50 mL), a series of TOCFs/CNTs suspensions with various TOCFs-to-CNTs ratios of 10:1, 15:1, 20:1, 25:1, and 30:1 can be obtained (designated as S01, S02, S03, S04, and S05, respectively). The conductive TOCFs/CNTs papers were then prepared by vacuum-assisted filtration (designated as TC01, TC02, TC03, TC04, and TC05, respectively). More details about the composition of the TOCFs/CNTs suspensions and the paper sensors are provided in Table S1. Besides, the thickness of the papers can be controlled by the amount of the TOCFs/CNTs suspension added. After drying, the conductive TOCFs/CNTs papers were cut into rectangular sheets with a size of 20 × 5 mm^2. The conductive silver paste was painted on both ends of the samples as contact electrodes, and the distance between the two electrodes was 10 mm. The obtained paper sensors were further vacuum dried overnight at 60 ℃ before testing.

2.5. Characterization

The morphology of the TOCFs before and after assembling CNTs was observed by an optical microscope (BX51, Olympus, Japan). The surface morphology and the elemental mapping of the conductive TOCFs/CNTs paper were characterized by a field scanning electron microscope (Merlin, Zeiss, Germany) in 5 kV. The contact angle of the samples was measured with 3 μL water droplets by using a contact angle meter (OCA40 Micro, Dataphysics, Germany). The Raman spectra of the samples were recorded by a Raman spectrometer (LabRAM Aramis, Jobin Yvon, France) equipped with a laser with an excitation wavelength of 532 nm. Fourier transform infrared spectra (FTIR, VERTEX 70, Bruker, Germany) of the samples were measured in the 3700–600 cm^{-1} range. The water vapor uptake of the samples was measured by water & organic vapor sorption analyzer (Aquadyne DVS-2HT, Quantachrome, USA).

2.6. Humidity sensing measurements

The various humidity conditions were produced by saturated solutions of different salts, and the relative humidity (RH) values were listed

below: LiCl (11%), $CaCl_2{\cdot}6H_2O$ (29%), K_2CO_3 (43%), $NaBr{\cdot}2H_2O$ (57%), NaCl (75%) and KNO_3 (95%). The sensor for the testing was hung in the sealed plastic bottle containing a saturated salt solution, and the two ends with silver paste electrodes were connected with an electrochemical workstation (CHI660E, CHI, China). The RH response of the sensor can be achieved by exposing the sensor in the bottles with different salts. The responsive properties were characterized by the change of current flowing through the sensor under an applied voltage of 1 V. The current–voltage (I-V) curves of the sensors were measured under dry silica gel atmosphere (0% RH). All the humidity sensitive performance tests were carried out at 25 ℃.

3. Results and discussion

In a typical process, CNTs were dispersed by using CTAB as a surfactant, which introduced cationic CTAB micelles on the surfaces of the CNTs, leading to positively charged CNTs. Conversely, due to the C6-hydroxyl groups on the cellulose fibers were selectively oxidized to

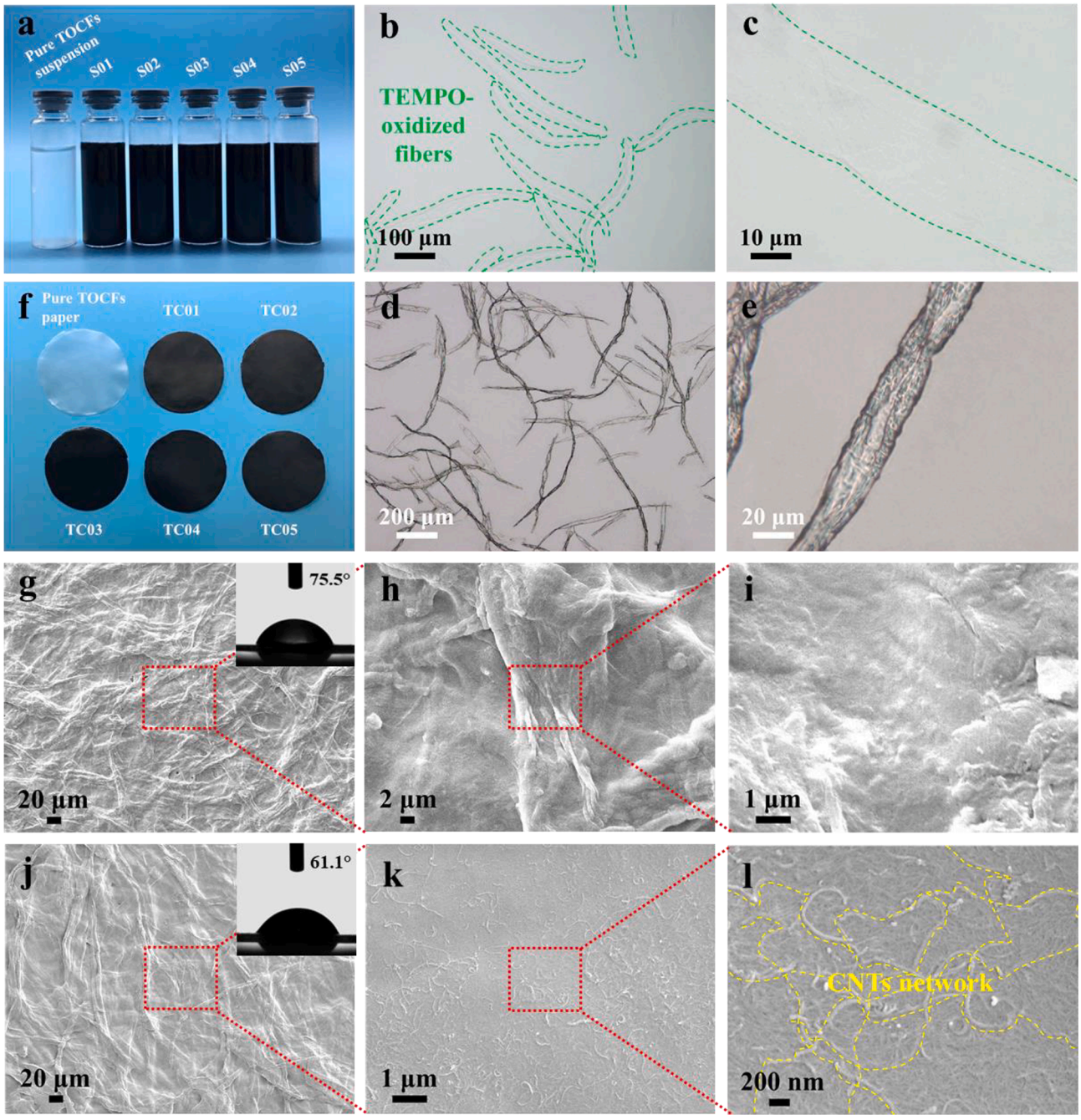

Fig. 2. Morphology characterization of the conductive cellulose fibers and the prepared paper sensor. (a) Photograph of pure TOCFs and TOCFs/CNTs suspensions. The TOCFs/CNTs suspensions with various TOCFs-to-CNTs ratios of 10:1, 15:1, 20:1, 25:1, and 30:1 were designated as S01, S02, S03, S04, and S05, respectively. Optical microscope images (b) and (c) show the translucent appearance of the TOCFs. Optical microscope images (d) and (e) show the appearance of the conductive TOCFs after assembling the CNTs in S01. (f) Photograph of pure TOCFs paper and the conductive papers with various TOCFs-to-CNTs ratios of 10:1, 15:1, 20:1, 25:1, and 30:1. SEM images (g), (h), and (i) show the rough network structure of the pure TOCFs paper. The inset in (g) illustrates the water contact angle of the pure TOCFs paper. (j) SEM image shows the smooth and closed surface morphology of TC01. The inset illustrates the water contact angle of TC01. SEM images (k) and (l) show continuous CNTs network adsorbed on the surface of TOCFs.

carboxyl groups in the process of TEMPO oxidization, strong negative charges were introduced to the surface of the fibers. CNTs can be tightly adsorbed on the surface of TOCFs by the electrostatic attraction. Therefore, a series of suspensions with various TOCFs-to-CNTs ratios of 10:1, 15:1, 20:1, 25:1, and 30:1 was obtained (Fig. 2a). The pure TOCFs suspension was also prepared and used as a control sample. Since the fibers were reduced to smaller size and swelling occurred as well during TEMPO oxidation treatment, the pure TOCFs suspension shows translucent. After assembling the CNTs, the TOCFs/CNTs suspensions turn to completely opaque. Notably, the fibers in S01 and S02 settle to the bottom of the container after standing for 24 h, while other suspensions remain stable (Fig. S1). It is because more CNTs were adsorbed on the fibers by electrostatic attraction in the suspensions with lower TOCFs content, resulting in a greater decrease in the negative charges of the TOCFs. This can be confirmed by the zeta potentials of the suspensions (Table S2). Besides, the adsorption of CNTs by TOCFs was further characterized by an optical microscope. As shown in Fig. 2b-c, the TOCFs are highly transparent and they are even not visible with eyes, whereas the conductive TOCFs are black because CNTs are firmly adsorbed on the TOCFs surface (Fig. 2d and Fig. S2). Moreover, at higher magnification, no obvious CNTs aggregation is observed (Fig. 2e).

The conductive TOCFs/CNTs papers with various TOCFs-to-CNTs ratios of 10:1, 15:1, 20:1, 25:1, and 30:1 can be obtained by vacuum-assisted filtration (Fig. 2f). SEM elemental mapping was performed to study the composition of the prepared samples. As shown in Fig. S3, the elemental mapping images demonstrate a homogenous distribution of C, O, Na, N, Br in the papers. The papers were then cut into small pieces with a size of 20 × 5 mm^2. The conductive silver paste was painted on both ends of the samples as contact electrodes. The prepared TC01 shows good flexibility with a curvature of 6.7 cm^{-1} (Fig. S4). Afterwards, the samples were connected to a circuit with a LED, respectively, the brightness of which indicates the electronic conductivity of the samples. Obviously, the conductivity of the papers increases with the CNTs loadings (Fig. S5). Fig. 2g-i show the morphology of the pure TOCFs paper, the cellulose fibers interweave with each other, forming a relatively rough network structure. Besides, due to the abundant hydroxyl groups existed on the cellulose fibers surface, the paper exhibits hydrophilic property with a contact angle of 75.5° (the inset in Fig. 2g). Meanwhile, the top-view morphology of TC01 was also studied. As shown in Fig. 2j-k, the surface of TC01 seems smoother than that of pure TOCFs paper. Higher magnification SEM image confirms that continuous CNTs network was adsorbed on the surface of the fibers (Fig. 2l), which leads to the smooth surface of TC01. Moreover, the uniform distribution of CNTs on the surface of the fibers further proves the homogeneous adsorption of CNTs by the negatively charged TOCFs in water. As a result, the conformal CNTs network on the surface of the fibers contributes to the high smoothness and excellent conductivity of TC01. On the other hand, because of the existence of CTAB in TC01, it shows a lower water contact angle than pure TOCFs paper (the inset in Fig. 2j).

The conductive TOCFs/CNTs paper was further investigated by the Raman spectrum and FTIR. As shown in Fig. 3a, the peak at 1346 cm^{-1} corresponds to the D-band, which is ascribed to defects and curvature in the nanotube lattice. And the peaks at 1579 cm^{-1} and 2690 cm^{-1} represent the G-band and 2D-band, respectively. They are induced by the in-plane vibration of the C − C bond [61]. The intensity ratio of the D-band and G-band (I_D/I_G) is commonly used to quantify the degree of defects in carbon materials. The I_D/I_G of CNTs is 0.67, while the value increases to 0.92 for TC01. The slight increase of the I_D/I_G value indicates that more defects were introduced in TC01. Due to the non-covalent interaction between CTAB and CNTs, it can be speculated that the increased defects were caused by ultrasonic treatment. To study the interaction between the CNTs and TOCFs, FTIR of the samples was also performed. As shown in Fig. 3b, the peak at 3440 cm^{-1} represents the stretching vibration of the O—H band of CNTs. The peaks located at 1636 and 1024 cm^{-1} are assigned to the stretching vibration of the C═O band and C—O band, respectively, suggesting the existence of —COOH on the CNTs surface. As for pure TOCFs paper and TC01, the peaks at 3330, 2907, 1597, and 1024 cm^{-1} stand for the stretching vibration of the O—H band, C—H band, C═O band, and C—O band, respectively. Compare to CNTs, the characteristic peaks of the O—H band and C═O band for the pure TOCFs paper and TC01 shift towards low frequency. Notably, the peak of O—H shifts from 3440 cm^{-1} to 3330 cm^{-1}, indicating that hydrogen bonding was formed not only between TOCFs but also between TOCFs and CNTs.

The humidity sensitive performance of the prepared paper sensors was evaluated by placing them under various RH conditions and the electrical signals were recorded by using an electrochemical workstation. Fig. 4a displays the current-voltage (I-V) curves of the sensors under 0% RH. They are linear over a wide range of voltage (-1 to 1 V), suggesting an ideal ohmic contact between the sensors and the two electrodes. Moreover, the dynamic response curves of the sensors through humidification-dehumidification cycles between 11% and 29, 43, 57, 75, and 95% RH were explored, as shown in Fig. 4b, in which the response of the sensors was expressed by means of the equation: Response = $-\Delta I/I_0$, where $\Delta I = I_{RH} - I_0$, I_0 is the initial current flowing through the samples at 11% RH; I_{RH} is the current upon exposure to the target RH conditions. As can be seen, all the samples are sensitive to the change of RH and demonstrate the highest response value at 95% RH, indicating that more water molecules can be adsorbed by the sensitive materials at high RH and lead to a greater response of the sensors. Note that the response of the sensors at 95% RH can be simply tailored from 37.1% to 80.9% by increasing the TOCFs/CNTs ratios from 10:1 to 30:1. This observation suggests the composition proportion of the TOCFs/

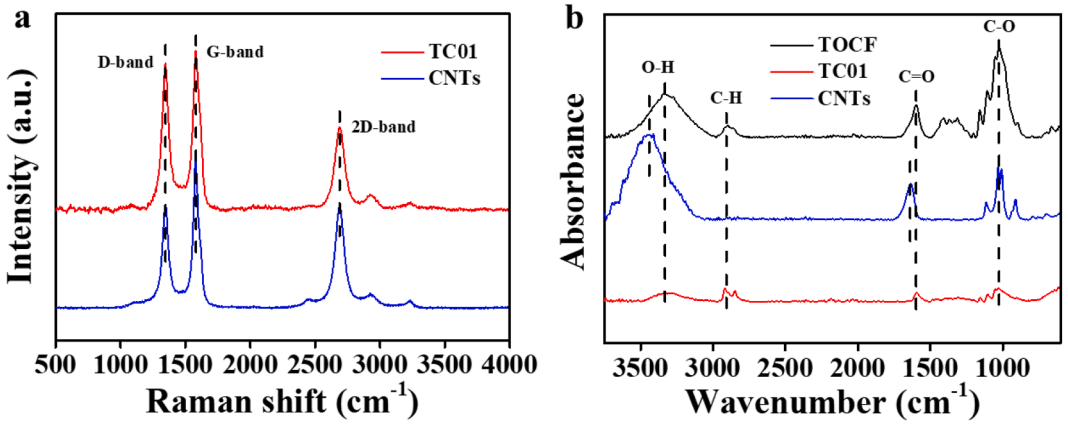

Fig. 3. (a) Raman spectra of TC01 and CNTs. (b) FTIR of the pure TOCFs paper, TC01, and CNTs.

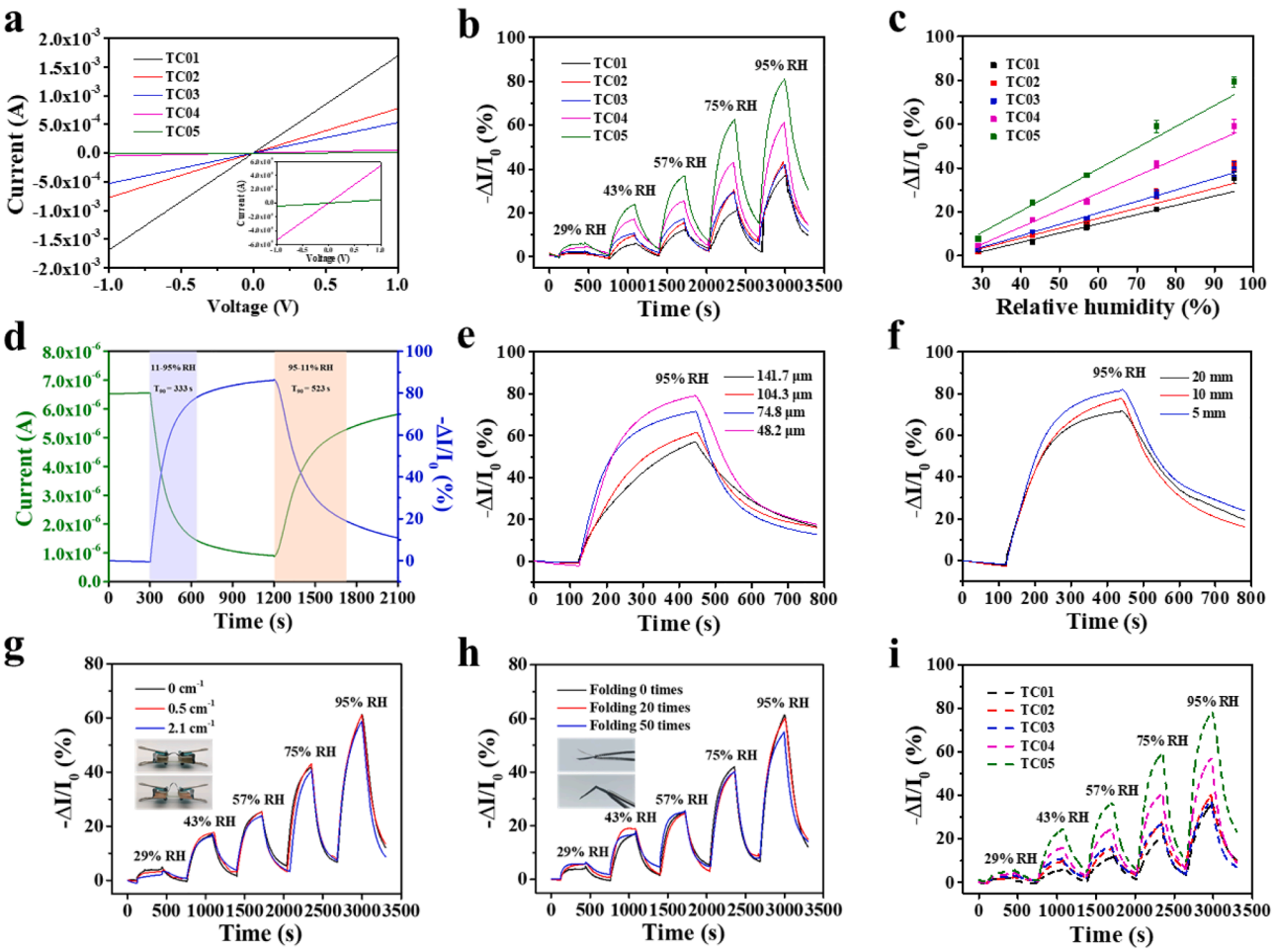

Fig. 4. Characterization of humidity sensitive performance of the obtained paper sensors. (a) Current-voltage (I-V) curves of the paper sensors with various TOCFs-to-CNTs ratios under dry environment. (b) Dynamic response and recovery curves of the paper sensors with various TOCFs-to-CNTs ratios between 11% and 29, 43, 57, 75, and 95% RH. (c) The response of the paper sensors with various TOCFs-to-CNTs ratios as a function of RH. (d) Response and recovery curve of TC05 between 11 and 95% RH. (e) The response of TC05 as a function of the thickness of the sensor. (f) The response of TC05 as a function of the distance between the two contact electrodes of the sensor. (g) Dynamic response and recovery curves of TC04 under various bending states. The inset illustrates the bending treatment. (h) Dynamic response and recovery curves of TC04 after folding for different number of times. The inset illustrates the folding treatment. (i) Dynamic response and recovery curves of the paper sensors with various TOCFs-to-CNTs ratios between 11% and 29, 43, 57, 75, and 95% RH measured after exposure to air for 3 months.

CNTs have a significant impact on the performance of the sensors, the low CNTs loading ratio drastically reduces the conductivity of TC05 closed to the percolation threshold, resulting in outstanding sensitive performance. Accordingly, we further increase the TOCFs-to-CNTs ratio to 35:1 to optimize the property of the sensor, but the current signal is too low and the response characteristic of p-type semiconductor CNTs disappears, suggesting the sample is an insulator (Fig. S6). Based on the above results, TC05 exhibits the highest sensitivity in our design. However, the baseline of the dynamic response curves of the sensors exhibits obvious drift, especially TC05. It is because the recovery speed of the sensors is slower than their response speed, some water molecules are accumulated on the sensitive materials during the recovery process, leading to unbalanced water adsorption and desorption cycles and gradually increased current baseline. By increasing the sampling time, the baseline drift can be greatly reduced (Fig. S7). Fig. 4c shows the responses of the sensors as a function of RH, the responses increase linearly with RH, indicating excellent linearity of the sensors.

Apart from the responsive property, the response and recovery times of the sensor were also measured by extending the sampling time to 15 min for the sensor to reach the equilibrium state. They are defined as the time taken by the sensor to achieve 90% of the total current change during the humidification-dehumidification process, respectively. As shown in Fig. 4d, the response value when TC05 reaches the saturation state is up to 87.0%, and the response and recovery times are calculated to be 333 and 523 s, respectively. Compare to other inorganic sensors, TC05 shows relatively slow response and recovery speed. This is due to the response mechanism of our sensor is based on the formation and breaking of hydrogen bonding. When the sensor was exposed to the humidity conditions, water molecules were primarily adsorbed by TOCFs via hydrogen bonding. To achieve the maximum response, more water molecules were captured by the sensitive materials to reach the saturation state, thereby leading to long response and recovery times. The slow response and recovery speeds make our sensor unfavorable, but for practical applications, the sensors are usually required to respond instantly to the change in RH instead of maximum response. For instance, TC05 demonstrates a superior responsive property to human breath even at a very rapid frequency, which will be discussed in detail in the last part of the paper. The hysteresis of the sensors was also measured by recording the current signal at various RH conditions after reaching equilibrium. As shown in Fig. S8, TC05 exhibits a hysteresis with a value of 7.3% at 57% RH.

The thickness of the sensors has an important effect on their humidity sensitive performance. To quantify the influence of the thickness on the sensing property of the sensors, the response curves of the sensors with different thicknesses (48.2 μm, 74.8 μm, 104.3 μm, and 141.7 μm) were measured (Fig. 4e). The result shows that as the thickness

decreases from 141.7 to 48.2 μm, the corresponding response value at 95% RH increases from 57.0% to 80.2%. This can be explained in three ways. (1) When the water molecules are adsorbed by the sensitive materials, water molecules will gradually penetrate from the surface of the sensor to the interior. At the same RH level, the penetration of water molecules is much easier in a thinner paper sensor than that in a thicker one. As a result, the thinner sensor shows a higher sensitivity. (2) The thicker sensor has more hole carriers as more CNTs containing, thereby the resistance of the thicker sensor will not increase as rapidly as the thinner sensor. (3) The swelling effect of TOCFs will be greatly restricted by the thicker structure, leading to the smaller expansion of the conductive CNTs network and decreased humidity sensitivity.

In addition, the sensitive performance of the sensors with various exposure areas of 20 × 5 mm^2, 10 × 5 mm^2, and 5 × 5 mm^2 was also investigated. With the increase of the distance between the two contact electrodes from 5 mm to 20 mm, the response value of the sensor gradually decreases (Fig. 4f). In fact, as the exposure part of the sensor increases, according to the formula $R = \rho^*L/S$, (where ρ, L, and S represent the electrical resistivity, length, and cross-sectional area of the sensor, respectively), the initial resistance of the sensor increases proportionally. Moreover, the sensor with a larger exposure part needs to adsorb more water molecules to achieve adsorption equilibrium, which causes the sensor cannot reach the response value of the smaller sensor in 5 min. Therefore, the humidity sensitivity of the sensors decreases with the increase of the exposure area.

The paper sensors demonstrate high sensitivity and excellent linearity as previously described, making them promising candidates for various humidity detecting applications. To better evaluate the practical application of the sensors, the sensitive performance of the paper sensor under bending and folding states was investigated. As shown in Fig. 4g and 4h, the response values of the sensor only show slight change before and after bending and folding treatment, indicating good bending and folding durability of the sensor. Furthermore, the long-time stability was also explored. The sensors were exposed to the air for 3 months, the dynamic response curves of the sensors were measured afterwards. Notably, no obvious change in the current signal of the samples is observed during the humidification-dehumidification cycles, which suggests the paper sensors have excellent stability (Fig. 4i).

Based on the above results, the prepared paper sensors exhibit a wide response range, high sensitivity, excellent linearity, superior bending and folding durability, and good long-time stability. In addition, compared with the sensors based on CNTs and cellulose materials reported in previous publications, our sensor shows the highest humidity sensitivity (Table 1).

The humidity sensitive behavior of the paper sensors was further investigated by using water & organic vapor sorption analyzer to elucidate the underlying mechanism. Fig. 5a shows the water vapor adsorption isotherm of the sensors at 25 ℃. As the results demonstrate, when RH is below 70%, the water vapor uptake of all samples is almost linear with RH. At this stage, the water molecules in the humidity condition are firstly adsorbed by the hydrophilic groups, such as hydroxyl groups, carboxyl groups, existed on the surface of the sensitive materials through hydrogen bonding, the adsorbed water molecules are unable to move freely due to the restriction from the two contiguous hydrogen bonding. Afterwards, multiple layers of water molecules are sequentially adsorbed on the first water molecules layer, and the outer water molecules layers are mobile because only one hydrogen bonding is formed locally (Fig. 5b). Moreover, at higher RH conditions, more water molecules can be adsorbed and further formed more partly free water molecules layers on the sensor, leading to higher water vapor uptake. At the second stage, when RH is greater than 70%, the adsorbed water molecules on the surface of the sensitive material have more freedom to move, and the capillary forces which bring about the capillary condensation of the less ordered water molecules layers in the voids of the sensor. As a result, the adsorption capacity of all samples significantly increases close to 25% at 90% RH.

In addition, it is worth noting that the sensors with various TOCFs-to-CNTs ratios show a negligible difference in water vapor adsorption performance, whereas the humidity sensitive performance of the sensors measured by the electrochemical workstation exhibits distinct difference (Fig. 4b). This can be explained as follows. The humidity sensitive materials of our sensors consist of CNTs and TOCFs. Due to the inherent hydrophobicity of CNTs, the water vapors adsorbed by CNTs can be ignored, and thus TOCFs play the main role in the adsorption of water molecules. Furthermore, except the loading ratio of CNTs, the exposure area and the thickness of the sensors are almost the same (Table S3), so the sensors display similar water vapor uptake under the various RH conditions (Fig. 5a). More importantly, the adsorbed water molecules can also cause the hydrophilic TOCFs to swell, as shown in Fig. S9. The swelling of the fibers will cause the hygroscopic expansion of the TOCFs/CNTs network and disrupt the conductive CNTs network, resulting in increased resistance of the paper sensors. Especially, compare with TC01, the conductive CNTs network of the sensors with lower CNTs loading is more susceptible to the swelling of TOCFs, which well explains the highest sensitivity of TC05 among the prepared sensors (Fig. 5c). Based on the above results, it can be concluded that the humidity sensitive performance of our sensors is dominated by the swelling of the TOCFs.

The prepared paper sensors exhibit excellent flexibility and high sensitivity. To evaluate the responsive performance of the sensors under

Table 1
Comparison of the performance of the humidity sensors based on CNTs and cellulose materials between this work and previous publications.

No.	Component	Output signal	RH range	Response	Response and recovery time	Hysteresis	Linearity	Ref.
1	COOH-functionalized SWCNTs coated paper	conductance	10–75% RH	37.5% ($\Delta S/S_0$)	6 s/200 s (10–60% RH)		linear	[63]
2	Functionalized MWCNTs coated paper	conductance	20–90% RH	61.0% ($\Delta G/G_0$)			linear	[64]
3	H_2SO_4 and HNO_3 (3:1) treated MWCNTs coated paper	current	11–95% RH	33.0% ($\Delta I/I_0$)	470 s/500 s	7.6% RH	linear	[65]
4	Regenerated cellulose/CNTs composite fiber	resistance	35–86% RH	44.0% ($\Delta R/R_0$)			nonlinear	[50]
5	Regenerated cellulose/CNTs composite film	resistance	35–86% RH	61.0% ($\Delta R/R_0$)			nonlinear	[61]
6	Nanofibrillated cellulose/MWCNTs composite film	current	11–95% RH	69.9% ($\Delta I/I_0$)	330 s/377 s	3.2% RH	linear	[62]
7	TEMPO-oxidized cellulose fibers/functionalized CNTs paper	current	11–95% RH	87.0% ($\Delta I/I_0$)[a]	333 s/523 s	7.3% RH	linear	our work

[a] The value is equivalent to 643.8% when the response of the sensor is expressed by $\Delta R/R_0$, where $\Delta R = R_{RH} - R_0$, R_0 is the initial resistance of the sensor at 11% RH; R_{RH} is the resistance of the sensor at the target RH conditions. It indicates that our sensor shows significantly enhanced sensitivity compare to the cellulose/CNTs sensors reported in previous publications.

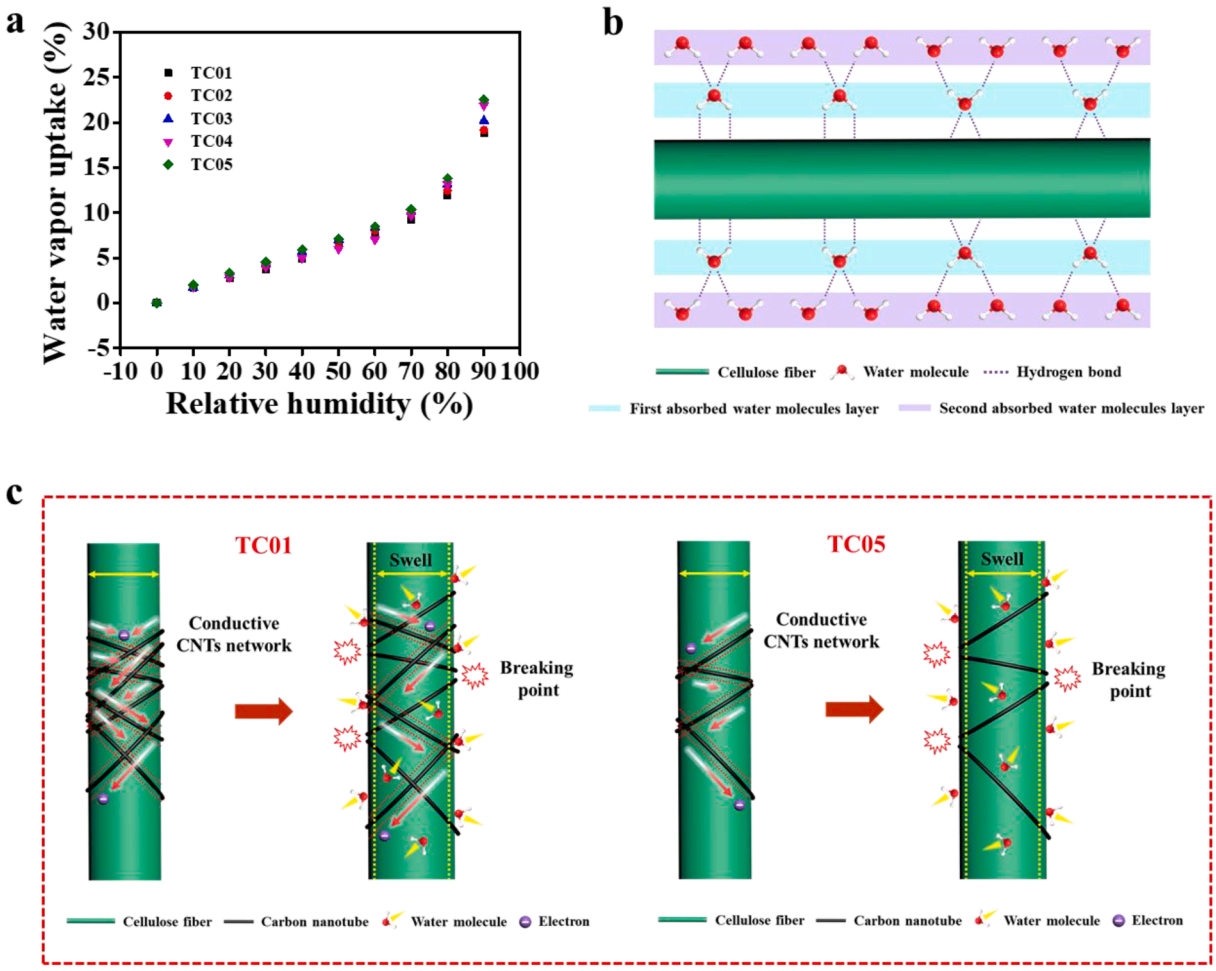

Fig. 5. Humidity sensitive mechanism of the paper sensors. (a) The water vapor adsorption isotherm of the paper sensors with various TOCFs-to-CNTs ratios at 25 ℃. (b) Schematic illustration of the adsorption of water molecules on the surface of the TOCFs. (c) Schematic illustrations of the conductive CNTs network of TC01 and TC05 destroyed by the swelling of the TOCFs.

the real working circumstance, TC05 was demonstrated to detect nose breathing and mouth breathing, as shown in Fig. 6a. During the respiratory process, the air containing water vapors exhaled from the nose or mouth can change the humidity around TC05, resulting in the variation of the current flowing through the sensor. Note that the current drops sharply in the initial stage. This is because the response speed of the sensor was faster than its recovery speed, which causes some water molecules to be trapped in the sensor after each response and recovery cycle. After 65 s, the sensor achieves adsorption and desorption equilibrium. Besides, for the mouth breathing curve, the current signal of TC05 shows greater change, indicating that more water molecules can be captured from the exhaled air by mouth. Fig. 6b shows the response of the sensor for detecting rapid breathing, normal breathing, and slow breathing, the breathing rate can be clearly distinguished from the number of peaks in the curves. Moreover, the air exhaled by the human body not only carries a lot of water vapors but also has a relatively high temperature. To study the influence of the temperature, the current–temperature curve of the sensor was measured (Fig. 6c). As can be seen, the current signal increases with the temperature in the range of 25 to 80 ℃. This can be explained by the semiconductor behavior of CNTs that the bandgap hinders the thermal activation of electrons from the valence to conduction states [61,66–68]. On the other hand, it is known that the conductivity of the sensor follows a negatively correlated relationship with humidity from the above studies, thereby it can be concluded that the humidity sensitivity rather than temperature sensitivity is responsible for the detecting of human respiration.

The sensor can also be applied to detect the humidity around the fingertip. Fig. 6d shows the variation of current with the distance between the fingertip and the sensor. When the fingertip approaches the sensor, the humidity around the sensor increases, resulting in a decrease of the current. In contrast, the current increases accordingly after the finger moves away. Also, the response value of the sensor becomes lower as the initial distance between the fingertip and the sensor increases. It is worth noting that the sensor shows a good response to the fingertip even at a distance of 1.0 cm, which demonstrates that the humidity sensor has good non-contact switching characteristics. Given the current spread of COVID-19, the sensor has potential application in untouched switches to decrease the risk of virus transmission.

TC05 was also used to detect changes in air humidity. Fig. 6e shows the humidity of air at different times of the day measured by TC05 and commercialized electronic hygrometer, respectively. Air humidity gradually decreases from morning to afternoon and reduces to a minimum value of 41% RH at around 14 o'clock, follows by increasing in the afternoon, but slightly decreasing at night (Fig. S10). For the humidity detecting by TC05, due to the conductivity of the sensor is negatively correlated with humidity, the variation trend of the current signal of TC05 is opposite to that measured by the commercialized electronic hygrometer, and thus the results of the above two methods are completely consistent. The accuracy of air humidity measured by TC05 was evaluated by converting the current signal into humidity by using the data in Fig. 4c. The differences between the converted humidity and the electronic hygrometer measured humidity are small and acceptable,

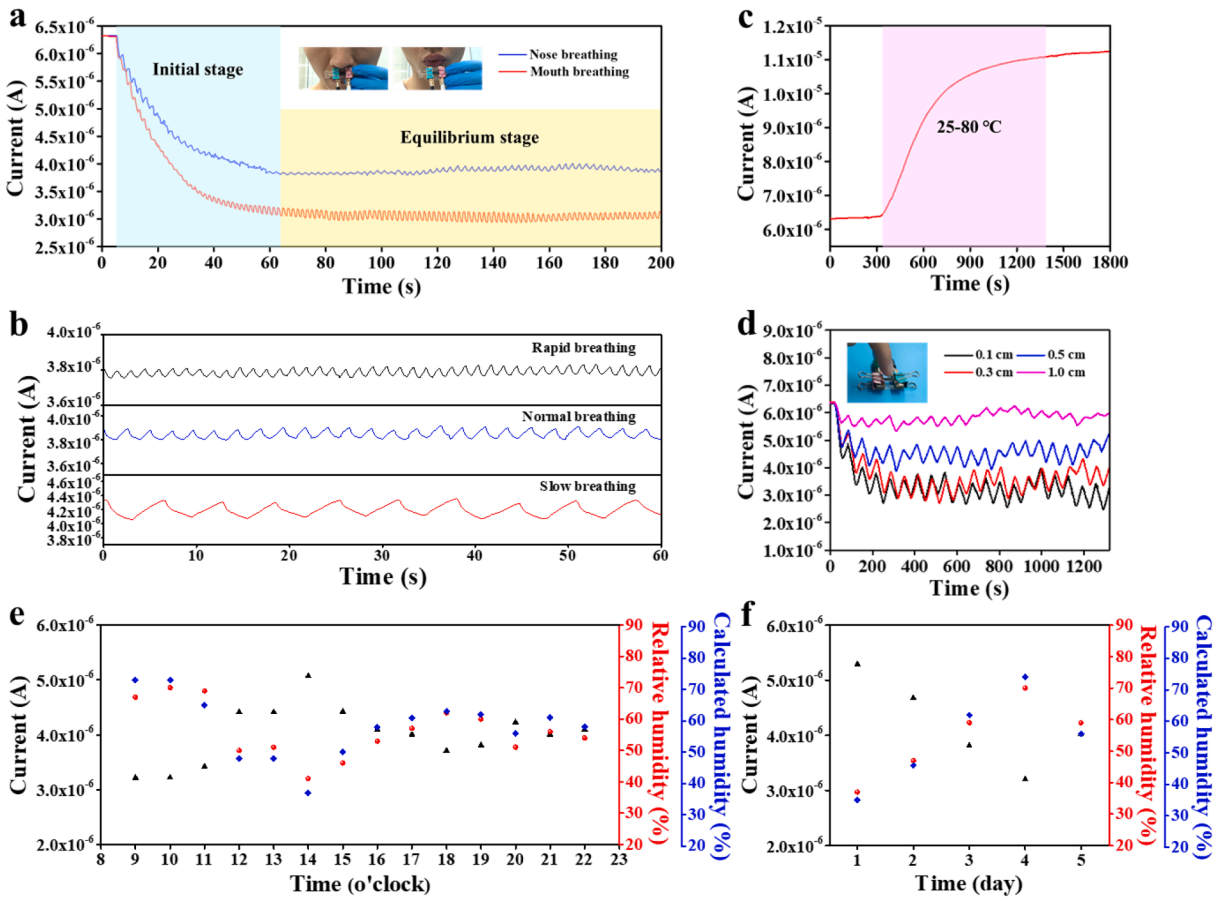

Fig. 6. Proof-of-concept demonstrations of the paper sensor for the applications in human breath, fingertip humidity, and air humidity monitoring. (a) Current-time curves of human nose breathing and mouth breathing. The inset illustrates the monitoring of nose breathing and mouth breathing using TC05. The temperature of nose breathing and mouth breathing is 33.6 ℃ and 36.8 ℃, respectively. (b) Current-time curves of human nose breathing at a rapid, normal, and slow frequency. (c) The current–temperature curve of TC05. (d) Current-time curves of the humidity around fingertip measured by TC05 with distances of 0.1 cm, 0.3 cm, 0.5 cm, and 1.0 cm, respectively. (e) Air humidity at different times of the day measured by TC05 and commercialized electronic hygrometer, respectively. (f) Air humidity at 10 o'clock measured by TC05 and commercialized electronic hygrometer in 5 days.

indicating the adaptability of TC05 for measuring air humidity. Furthermore, the test cycle was extended to 5 days and air humidity was measured by TC05 and the electronic hygrometer at 10 o'clock, 14 o'clock, 18 o'clock, and 22 o'clock every day (Fig. 6f, Fig. S11 and S12). The results show that the actual air humidity in these 5 days can be well recorded by TC05. Therefore, the sensors we prepared demonstrate the possibility for the applications in various humidity measurements.

4. Conclusions

In conclusion, we developed a flexible paper-based humidity sensor where CTAB-dispersed CNTs can be firmly adsorbed on the surface of negatively charged TOCFs through electrostatic attraction. Owing to the excellent hydrophilicity of TOCFs and the rational structure design of TOCFs/CNTs conformal fibers network, the sensor exhibited an outstanding humidity sensitive response of 87.0% ($\Delta I/I_0$, and the response limit is 100%) at 95% RH. Besides, the sensor also displayed excellent linearity ($R^2 = 0.995$) over the measured humidity range from 11 to 95% RH, superior bending (with a curvature of 2.1 cm^{-1}) and folding (up to 50 times) durability, and good long-time stability (more than 3 months). As a proof of concept, the sensor has been demonstrated to monitor human respiration, fingertip humidity, and air humidity, indicating its promising applications in various humidity measurements.

Declaration of Competing Interest

The authors declare that they have no known competing financial interests or personal relationships that could have appeared to influence the work reported in this paper.

Acknowledgements

Gang Chen acknowledges the support of the State Key Laboratory of Pulp and Paper Engineering at South China University of Technology (2020ZD02) and National Key Research and Development Program (2018YFC1902102). Yudi Kuang acknowledges the financial support from China Postdoctoral Science Foundation (2019M662925). Penghui Zhu acknowledges the financial support of the China Scholarship Council (201906150070).

Appendix A. Supplementary data

Supplementary data to this article can be found online at https://doi.org/10.1016/j.cej.2020.127105.

References

[1] Y. Su, J. Wang, B. Wang, T. Yang, B. Yang, G. Xie, Y. Zhou, S. Zhang, H. Tai, Z. Cai, Alveolus-inspired active membrane sensors for self-powered wearable chemical sensing and breath analysis, ACS Nano 14 (2020) 6067–6075.

[2] Y. Su, M. Yao, G. Xie, H. Pan, H. Yuan, M. Yang, H. Tai, X. Du, Y. Jiang, Improving sensitivity of self-powered room temperature NO2 sensor by triboelectric-photoelectric coupling effect, Appl. Phys. Lett. 115 (2019), 073504.

[3] Y. Su, G. Xie, H. Tai, S. Li, B. Yang, S. Wang, Q. Zhang, H. Du, H. Zhang, X. Du, Self-powered room temperature NO2 detection driven by triboelectric nanogenerator under UV illumination, Nano Energy 47 (2018) 316–324.

[4] T. Zhong, H. Guan, Y. Dai, H. He, L. Xing, Y. Zhang, X. Xue, A self-powered flexibly-arranged gas monitoring system with evaporating rainwater as fuel for building atmosphere big data, Nano Energy 60 (2019) 52–60.

[5] Y. Su, T. Yang, X. Zhao, Z. Cai, G. Chen, M. Yao, K. Chen, M. Bick, J. Wang, S. Li, A wireless energy transmission enabled wearable active acetone biosensor for non-invasive prediabetes diagnosis, Nano Energy 74 (2020), 104941.

[6] S. Wang, Y. Jiang, H. Tai, B. Liu, Z. Duan, Z. Yuan, H. Pan, G. Xie, X. Du, Y. Su, An integrated flexible self-powered wearable respiration sensor, Nano Energy 63 (2019), 103829.

[7] Y. Fu, H. He, T. Zhao, Y. Dai, W. Han, J. Ma, L. Xing, Y. Zhang, X. Xue, A self-powered breath analyzer based on PANI/PVDF piezo-gas-sensing arrays for potential diagnostics application, Nano-micro Lett. 10 (2018) 76.

[8] T. Zhong, M. Zhang, Y. Fu, Y. Han, H. Guan, H. He, T. Zhao, L. Xing, X. Xue, Y. Zhang, An artificial triboelectricity-brain-behavior closed loop for intelligent olfactory substitution, Nano Energy 63 (2019), 103884.

[9] S. Xia, S. Song, G. Gao, Robust and flexible strain sensors based on dual physically cross-linked double network hydrogels for monitoring human-motion, Chem. Eng. J. 354 (2018) 817–824.

[10] Q. Zhang, X. Liu, L. Duan, G. Gao, Ultra-stretchable wearable strain sensors based on skin-inspired adhesive, tough and conductive hydrogels, Chem. Eng. J. 365 (2019) 10–19.

[11] Y. Ye, Y. Zhang, Y. Chen, X. Han, F. Jiang, Cellulose Nanofibrils Enhanced, Strong, Stretchable, Freezing-Tolerant Ionic Conductive Organohydrogel for Multi-Functional Sensors, Adv. Functl. Mater. (2020) 2003430.

[12] D. Zhang, Z. Xu, Z. Yang, X. Song, High-performance flexible self-powered tin disulfide nanoflowers/reduced graphene oxide nanohybrid-based humidity sensor driven by triboelectric nanogenerator, Nano Energy 67 (2020), 104251.

[13] R.N. Jenjeti, R. Kumar, S. Sampath, Two-dimensional, few-layer NiPS 3 for flexible humidity sensor with high selectivity, J. Mater. Chem. A 7 (2019) 14545–14551.

[14] C. Wang, K. Xia, H. Wang, X. Liang, Z. Yin, Y. Zhang, Advanced carbon for flexible and wearable electronics, Adv. Mater. 31 (2019) 1801072.

[15] J. Wu, Y.-M. Sun, Z. Wu, X. Li, N. Wang, K. Tao, G.P. Wang, Carbon nanocoil-based fast-response and flexible humidity sensor for multifunctional applications, ACS Appl. Mater. Interfaces 11 (2019) 4242–4251.

[16] J. Zhao, N. Li, H. Yu, Z. Wei, M. Liao, P. Chen, S. Wang, D. Shi, Q. Sun, G. Zhang, Highly sensitive MoS2 humidity sensors array for noncontact sensation, Adv. Mater. 29 (2017) 1702076.

[17] S.Y. Park, Y.H. Kim, S.Y. Lee, W. Sohn, J.E. Lee, Y.-S. Shim, K.C. Kwon, K.S. Choi, H.J. Yoo, J.M. Suh, Highly selective and sensitive chemoresistive humidity sensors based on rGO/MoS 2 van der Waals composites, J. Mater. Chem. A 6 (2018) 5016–5024.

[18] J. Yang, R. Shi, Z. Lou, R. Chai, K. Jiang, G. Shen, Flexible Smart Noncontact Control Systems with Ultrasensitive Humidity Sensors, Small 15 (2019) 1902801.

[19] H. Wang, S. Li, Y. Wang, H. Wang, X. Shen, M. Zhang, H. Lu, M. He, Y. Zhang, Bioinspired Fluffy Fabric with In Situ Grown Carbon Nanotubes for Ultrasensitive Wearable Airflow Sensor, Adv. Mater. 32 (2020) 1908214.

[20] J. Zhao, L. Li, Y. Zhang, C. Li, Q. Zhang, J. Peng, X. Zhao, Q. Li, X. Wang, J. Xie, Novel coaxial fiber-shaped sensing system integrated with an asymmetric supercapacitor and a humidity sensor, Energy Storage Mater. 15 (2018) 315–323.

[21] J. Gao, L. Wang, Z. Guo, B. Li, H. Wang, J. Luo, X. Huang, H. Xue, Flexible, superhydrophobic, and electrically conductive polymer nanofiber composite for multifunctional sensing applications, Chem. Eng. J. 381 (2020), 122778.

[22] U. Kalsoom, S. Waheed, B. Paull, Fabrication of Humidity Sensor Using 3D Printable Polymer Composite Containing Boron-Doped Diamonds and LiCl, ACS Appl. Mater. Interfaces 12 (2020) 4962–4969.

[23] H. Qi, E. Mäder, J. Liu, Unique water sensors based on carbon nanotube–cellulose composites, Sens. Actuators, B 185 (2013) 225–230.

[24] H. Qi, J. Liu, Y. Deng, S. Gao, E. Mäder, Cellulose fibres with carbon nanotube networks for water sensing, J. Mater. Chem. A 2 (2014) 5541–5547.

[25] H. Qi, J. Liu, J. Pionteck, P. Pötschke, E. Mäder, Carbon nanotube–cellulose composite aerogels for vapour sensing, Sens. Actuators, B 213 (2015) 20–26.

[26] M. Castro, B. Kumar, J.-F. Feller, Z. Haddi, A. Amari, B. Bouchikhi, Novel e-nose for the discrimination of volatile organic biomarkers with an array of carbon nanotubes (CNT) conductive polymer nanocomposites (CPC) sensors, Sens. Actuators, B 159 (2011) 213–219.

[27] T. Villmow, S. Pegel, A. John, R. Rentenberger, P. Pötschke, Liquid sensing: smart polymer/CNT composites, Mater. Today 14 (2011) 340–345.

[28] P.-G. Su, J.-Y. Tseng, Y.-C. Huang, H.-H. Pan, P.-C. Li, Novel fully transparent and flexible humidity sensor, Sens. Actuators, B 137 (2009) 496–500.

[29] K. Parikh, K. Cattanach, R. Rao, D.-S. Suh, A. Wu, S.K. Manohar, Flexible vapour sensors using single walled carbon nanotubes, Sens. Actuators, B 113 (2006) 55–63.

[30] J. Covington, J. Gardner, D. Briand, N. De Rooij, A polymer gate FET sensor array for detecting organic vapours, Sens. Actuators, B 77 (2001) 155–162.

[31] K.-P. Yoo, L.-T. Lim, N.-K. Min, M.J. Lee, C.J. Lee, C.-W. Park, Novel resistive-type humidity sensor based on multiwall carbon nanotube/polyimide composite films, Sens. Actuators, B 145 (2010) 120–125.

[32] Q.-Y. Tang, Y. Chan, K. Zhang, Fast response resistive humidity sensitivity of polyimide/multiwall carbon nanotube composite films, Sens. Actuators, B 152 (2011) 99–106.

[33] J.-R. Cha, M.-S. Gong, Preparation of epoxy/polyelectrolyte IPNs for flexible polyimide-based humidity sensors and their properties, Sens. Actuators, B 178 (2013) 656–662.

[34] H. Yu, T. Cao, L. Zhou, E. Gu, D. Yu, D. Jiang, Layer-by-layer assembly and humidity sensitive behavior of poly (ethyleneimine)/multiwall carbon nanotube composite films, Sens. Actuators, B 119 (2006) 512–515.

[35] P. Tian, X. Gao, G. Wen, L. Zhong, Z. Wang, Z. Guo, Novel fabrication of polymer/carbon nanotube composite coated Janus paper for humidity stress sensor, J. Colloid Interface Sci. 532 (2018) 517–526.

[36] D. Wang, Y. Huang, W. Cai, M. Tian, P. Liu, Y. Zhang, Functionalized multi-wall carbon nanotubes/silicone rubber composite as capacitive humidity sensor, J. Appl. Polym. Sci. 131 (2014) 40342.

[37] Q.F. Ma, Z.Q. Tou, K. Ni, Y.Y. Lim, Y.F. Lin, Y.R. Wang, M.H. Zhou, F.F. Shi, L. Niu, X.Y. Dong, Carbon-nanotube/Polyvinyl alcohol coated thin core fiber sensor for humidity measurement, Sens. Actuators, B 257 (2018) 800–806.

[38] T. Fei, K. Jiang, F. Jiang, R. Mu, T. Zhang, Humidity switching properties of sensors based on multiwalled carbon nanotubes/polyvinyl alcohol composite films, J. Appl. Polym. Sci. 131 (2014) 39726.

[39] P.G. Ramos, N.J. Morales, S. Goyanes, R.J. Candal, J. Rodríguez, Moisture-sensitive properties of multi-walled carbon nanotubes/polyvinyl alcohol nanofibers prepared by electrospinning electrostatically modified method, Mater. Lett. 185 (2016) 278–281.

[40] W. Li, F. Xu, L. Sun, W. Liu, Y. Qiu, A novel flexible humidity switch material based on multi-walled carbon nanotube/polyvinyl alcohol composite yarn, Sens. Actuators, B 230 (2016) 528–535.

[41] S. Mallick, Z. Ahmad, F. Touati, J. Bhadra, R. Shakoor, N. Al-Thani, PLA-TiO2 nanocomposites: Thermal, morphological, structural, and humidity sensing properties, Ceram. Int. 44 (2018) 16507–16513.

[42] A. Bouvree, J.-F. Feller, M. Castro, Y. Grohens, M. Rinaudo, Conductive polymer nano-biocomposites (CPC): chitosan-carbon nanoparticle a good candidate to design polar vapour sensors, Sens. Actuators, B 138 (2009) 138–147.

[43] J. Xu, M. Bertke, X. Li, H. Mu, H. Zhou, F. Yu, G. Hamdana, A. Schmidt, H. Bremers, E. Peiner, Fabrication of ZnO nanorods and Chitosan@ ZnO nanorods on MEMS piezoresistive self-actuating silicon microcantilever for humidity sensing, Sens. Actuators, B 273 (2018) 276–287.

[44] H. Qi, E. Mäder, J. Liu, Electrically conductive aerogels composed of cellulose and carbon nanotubes, J. Mater. Chem. A 1 (2013) 9714–9720.

[45] L. Wang, K. Wang, Z. Lou, K. Jiang, G. Shen, Plant-based modular building blocks for “green” electronic skins, Adv. Funct. Mater. 28 (2018) 1804510.

[46] A.T. Vicente, A. Araújo, M.J. Mendes, D. Nunes, M.J. Oliveira, O. Sanchez-Sobrado, M.P. Ferreira, H. Águas, E. Fortunato, R. Martins, Multifunctional cellulose-paper for light harvesting and smart sensing applications, J. Mater. Chem. C 6 (2018) 3143–3181.

[47] M.M. Pérez-Madrigal, M.G. Edo, C. Alemán, Powering the future: application of cellulose-based materials for supercapacitors, Green Chem. 18 (2016) 5930–5956.

[48] H. Zhu, W. Luo, P.N. Ciesielski, Z. Fang, J. Zhu, G. Henriksson, M.E. Himmel, L. Hu, Wood-derived materials for green electronics, biological devices, and energy applications, Chem. Rev. 116 (2016) 9305–9374.

[49] C. Chang, L. Zhang, Cellulose-based hydrogels: Present status and application prospects, Carbohydr. Polym. 84 (2011) 40–53.

[50] H. Qi, B.r. Schulz, T. Vad, J. Liu, E. Mäder, G. Seide, T. Gries, Novel carbon nanotube/cellulose composite fibers as multifunctional materials, ACS Appl. Mater. Interf. 7 (2015) 22404-22412.

[51] Y. Su, G. Xie, S. Wang, H. Tai, Q. Zhang, H. Du, H. Zhang, X. Du, Y. Jiang, Novel high-performance self-powered humidity detection enabled by triboelectric effect, Sens. Actuators, B 251 (2017) 144–152.

[52] M. Tang, C. Zhang, J.-Y. Zhang, Q.-L. Zhao, Z.-L. Hou, K.-T. Zhan, Ultrafast-Response Humidity Sensor with High Humidity Durability Based on a Freestanding Film of Graphene Oxide Supramolecular, Phys. Status Solidi (a) 217 (2020) 1900869.

[53] S. Borini, R. White, D. Wei, M. Astley, S. Haque, E. Spigone, N. Harris, J. Kivioja, T. Ryhanen, Ultrafast graphene oxide humidity sensors, ACS Nano 7 (2013) 11166–11173.

[54] K.-L. Zhang, Z.-L. Hou, B.-X. Zhang, Q.-L. Zhao, Highly sensitive humidity sensor based on graphene oxide foam, Appl. Phys. Lett. 111 (2017), 153101.

[55] X. Ni, J. Luo, R. Liu, X. Liu, A novel flexible UV-cured carbon nanotube composite film for humidity sensing, Sens. Actuators, B 297 (2019), 126785.

[56] C. Chen, X. Wang, M. Li, Y. Fan, R. Sun, Humidity sensor based on reduced graphene oxide/lignosulfonate composite thin-film, Sens. Actuators, B 255 (2018) 1569–1576.

[57] G. Zhou, J.-H. Byun, Y. Oh, B.-M. Jung, H.-J. Cha, D.-G. Seong, M.-K. Um, S. Hyun, T.-W. Chou, Highly sensitive wearable textile-based humidity sensor made of high-strength, single-walled carbon nanotube/poly (vinyl alcohol) filaments, ACS Appl. Mater. Interfaces 9 (2017) 4788–4797.

[58] L. Liu, X. Ye, K. Wu, R. Han, Z. Zhou, T. Cui, Humidity sensitivity of multi-walled carbon nanotube networks deposited by dielectrophoresis, Sensors 9 (2009) 1714–1721.

[59] J.N. Coleman, U. Khan, W.J. Blau, Y.K. Gun’ko, Small but strong: a review of the mechanical properties of carbon nanotube–polymer composites, Carbon 44 (2006) 1624-1652.

[60] C. Cao, C. Hu, L. Fang, S. Wang, Y. Tian, C. Pan, Humidity sensor based on multi-walled carbon nanotube thin films, J. Nanomater. 2011 (2011), 707303.

[61] H. Qi, J. Liu, S. Gao, E. Mäder, Multifunctional films composed of carbon nanotubes and cellulose regenerated from alkaline–urea solution, J. Mater. Chem. A 1 (2013) 2161–2168.

[62] P. Zhu, Y. Liu, Z. Fang, Y. Kuang, Y. Zhang, C. Peng, G. Chen, Flexible and highly sensitive humidity sensor based on cellulose nanofibers and carbon nanotube composite film, Langmuir 35 (2019) 4834–4842.
[63] J.-W. Han, B. Kim, J. Li, M. Meyyappan, Carbon nanotube based humidity sensor on cellulose paper, J. Phys. Chem. C 116 (2012) 22094–22097.
[64] L. Xie, Y. Feng, M. Mäntysalo, Q. Chen, L.-R. Zheng, Integration of f-MWCNT sensor and printed circuits on paper substrate, IEEE Sens. J. 13 (2013) 3948–3956.
[65] H. Zhao, T. Zhang, R. Qi, J. Dai, S. Liu, T. Fei, Drawn on paper: a reproducible humidity sensitive device by handwriting, ACS Appl. Mater. Interfaces 9 (2017) 28002–28009.
[66] B. Wei, R. Spolenak, P. Kohler-Redlich, M. Rühle, E. Arzt, Electrical transport in pure and boron-doped carbon nanotubes, Appl. Phys. Lett. 74 (1999) 3149–3151.
[67] A. Kaiser, G. Düsberg, S. Roth, Heterogeneous model for conduction in carbon nanotubes, Physical Review B 57 (1998) 1418.
[68] V. Skákalová, A.B. Kaiser, Y.-S. Woo, S. Roth, Electronic transport in carbon nanotubes: From individual nanotubes to thin and thick networks, Phys. Rev. B 74 (2006), 085403.